HAL
open science

Experimental determination of the H–Hf phase diagram using in situ neutron diffraction

Maxime Dottor, Jean-Claude Crivello, L. Laversenne, Jean-Marc Joubert

To cite this version:

Maxime Dottor, Jean-Claude Crivello, L. Laversenne, Jean-Marc Joubert. Experimental determination of the H–Hf phase diagram using in situ neutron diffraction. Journal of Alloys and Compounds, 2023, 937, pp.168353. 10.1016/j.jallcom.2022.168353 . hal-04246782

HAL Id: hal-04246782

https://hal.science/hal-04246782v1

Submitted on 17 Oct 2023

HAL is a multi-disciplinary open access archive for the deposit and dissemination of scientific research documents, whether they are published or not. The documents may come from teaching and research institutions in France or abroad, or from public or private research centers.

L'archive ouverte pluridisciplinaire **HAL**, est destinée au dépôt et à la diffusion de documents scientifiques de niveau recherche, publiés ou non, émanant des établissements d'enseignement et de recherche français ou étrangers, des laboratoires publics ou privés.

Experimental determination of the H–Hf phase diagram using *in situ* neutron diffraction

Maxime Dottor[a], Jean-Claude Crivello[a], Laetitia Laversenne[b], Jean-Marc Joubert[a,]*

[a] Univ Paris Est Creteil, CNRS, ICMPE, UMR 7182, 2 rue Henri Dunant, 94320 Thiais, France

[b] University Grenoble Alpes, CNRS, Grenoble INP, Institut Néel, 38000 Grenoble, France

[*] Corresponding author. jean-marc.joubert@cnrs.fr

Abstract

The Hf–H(D) system was studied using *in situ* neutron diffraction as a function of composition (up to 2 D/Hf) and temperature (up to 900°C). This allowed to complement the previous knowledge about this system, in particular from the points of view of the phase existence and of the phase diagram. Two major findings are: the observation of a new phase (γ, PtS structure type) of composition HfH similar to the monohydride found in H–Zr system, in accordance with previous first-principles calculations, and the structure determination of the δ' phase (new structure type), an ordered superstructure of the δ phase (CaF_2 structure type). Phase relations are established, and a new phase diagram is proposed.

Keywords: D–Hf; H–Hf; Phase diagram; metal hydrides; neutron diffraction.

1. Introduction

The system H–Hf is interesting in particular because of its similarities and differences with H–Zr system. Hafnium, despite his price, has been recently considered as an important alloying element in hydrogen storage alloys [1]. It may also have application in hydrogen sensors [2]. Finally, in new generation nuclear reactors, hafnium hydrides are considered to be good candidates for control bars due to their specific neutron absorption properties [3-6]. For all these applications, the knowledge of H–Hf phase diagram is of primary importance. However, the phase diagram is only partially known. In particular, phase transformations and the crystal structures of all phases are not clearly established. Moreover, a new phase – the monohydride HfH – has been recently predicted by electronic density functional theory (DFT) calculations [7] but never seen experimentally. This system has therefore been reinvestigated experimentally in particular with the use of *in situ* neutron diffraction (ND) [8].

2. Bibliographic study

2.1. Phase diagram data

At least, four phases exist in the system: the hexagonal α-Hf (*hP*2, Mg, $P6_3/mmc$) solid solution and the different hydrides, the deformed cubic δ'-HfH_{2-x} with an unknown structure, the cubic δ-HfH_{2-x} (*cF*12, CaF_2, $Fm\bar{3}m$) and the tetragonal ε-HfH_2 (*tI*6, ThH_2, $I4/mmm$), see Table 1. The α, δ and ε phases were identified by ND [9, 10]. The phase transformation from α to β-Hf (*bcc*, *cI*2, W, $Im\bar{3}m$) occurs at 1743°C [11], far above the temperature range considered in the present study. Therefore, the β phase is not considered in this work. As for the liquid phase, due to the high temperature, no hydrogen solubility data is available.

From first-principles calculations, Bourgeois *et al.* [7] predicted the stabilization, at least at low temperature, of a phase of composition HfH (γ) with either PtS or NbH structure. It appears on the calculated ground state. This phase is similar to that present in the H–Zr system [12] but has never been reported in the H–Hf system.

The phase diagram has been studied by different authors using X-ray diffraction (XRD) essentially [13-15]. Due to the structural similarities between δ and ε phases, the transformation between the two phases may be of the first or the second order. Recently, Bannenberg *et al.* concluded in favor of a first order reaction for the bulk material while second order is observed for thin films [16].

The different studies on the δ' phase [13, 17-21] could conclude that it is related to the δ phase with a tetragonal distortion. First-principles calculation demonstrates that vacancy ordering is energetically favorable [20].

Zirconium is always present in Hf as an impurity (between 1 and 4 wt.% in the different reports). However, according to the different isothermal sections available on the ternary H–Hf–Zr system [22], the effect of zirconium on the different equilibria is quite limited. Oxygen, on the other hand, tends to decrease the hydrogen solubility in the material [23].

Table 1. Structural data of the known phases of the Hf–H phase diagram: α-Hf, δ'-HfH_{2-x}, δ-HfH_{2-x} and ε-HfH_2 [9, 10].

Phase	Protype	Lattice constants (Å)	Atom	*x*	*y*	*z*	Site
α-Hf	Mg, $P6_3/mmc$	a = 3.19, c = 5.05	Hf	1/3	2/3	1/4	2*c*
δ'-HfH_{2-x}	Unknown	a = 4.698, c = 4.672	-	-	-	-	-
δ-HfH_{2-x}	CaF_2, $Fm\bar{3}m$	a = 4.708	H Hf	1/4 0	1/4 0	1/4 0	8*c* 4*a*
ε-HfH_2	ThH_2, $I4/mmm$	a = 3.478, c = 4.361	H Hf	0 0	1/2 0	1/4 0	4*d* 2*a*

2.2. Thermodynamic data

Pressure-composition curves measured by the Sieverts' method are reported [2, 24-28]. They show a single plateau corresponding to the α-δ transformation without noticeable hysteresis. The limit between α and α+δ is not as sharp as that between α+δ and δ.

Isotopic effect by replacing hydrogen by deuterium has been studied in the solubility range of the α phase in Ref. [29]. In the full range of concentration, by calorimetric measurement of the partial enthalpies, no difference can be detected between hydrogen and deuterium at 334 K [28].

Calorimetric data is also available in Ref. [18] and isobaric data at 1 bar are reported by Espagno *et al.* [30].

3. Methodology

3.1. Experimental studies

High purity hafnium powder was used (Alfa Aesar, 99.6%, 2.49 wt.% Zr, 3300 ppm O). Both *ex* and *in situ* experiments were conducted and, depending on the experiment, either hydrogen or deuterium was used (deuterium was always used for ND experiments).

The ND measurement was carried out at the Institut Laue Langevin on D1B instrument (multi-detector containing 1280 cells, step size 0.1°, 2θ range 6-127°, for practical details see https://www.ill.eu/users/instruments/instruments-list/d1b/description/instrument-layout). The sample was connected to a hydrogenation device using the Sieverts' method allowing the monitoring of the deuterium quantity in the sample placed in a furnace. The temperature was measured as close as possible to the sample. The Sieverts' apparatus was also connected to a rotary pump that could also be used to desorb the sample (limit vacuum $5x10^{-2}$ mbar). We could therefore perform our *in*

situ study as a function of both temperature and composition. Since oxygen level plays a role in the equilibrium of the D–Hf phase diagram, the sample holders were filled with hafnium in an argon-filled glove box. We measured both samples previously prepared in our laboratory and samples that were deuterated on site in equilibrium state (typical time to reach equilibrium was 5-10 minutes) for an acquisition time between 10 and 30 minutes.

Two types of sample holders were used: silica for the high temperature measurements at pressure below 1 bar (inner diameter 6 mm) and stainless steel container at pressures up to 25 bar with a temperature limited to 500°C (inner diameter 6.92 mm).

The structural analysis was conducted using the Rietveld method (program Fullprof). The wavelength (1.278437 Å) was calibrated on a $Na_2Ca_3Al_2F_{14}$ sample. The linear absorption coefficient of the sample (hafnium neutron absorption is significant) was considered (μR values between 0.45 and 0.52). The background was interpolated between given points. The different phases were taken into account. Phase amount, lattice parameters, line widths, deuterium site occupancies and isotropic displacement parameters (distinct parameters for Hf and D) were refined when the phase was in a sufficiently significant amount.

In this work, several hydrides and deuterated samples were prepared using a Sieverts' type apparatus in our laboratory facility. After the hydrogenation / deuteration, the samples were characterized using a Bruker D8 Advance Bragg-Brentano diffractometer, using Cu-Kα radiation and a graphite monochromator in the diffracted beam. The Rietveld method [31] using the Fullprof package [32] was used to refine all the patterns. The structure of the δ' phase was solved using Fox software [33].

3.2. First-principles calculations

First-principles calculations were made in the same conditions as our previous study on this system [7], in the frame of the DFT using pseudopotential approach implemented in VASP code and PBE [34-36] functional. A cutoff of 800 eV was used for the plane wave basis set and a dense grid of k-points in the irreducible wedge of the Brillouin zone was generated with the Monkhorst−Pack [37] scheme. The heat of formation corresponding to the hydride formation at 0 K was calculated from the total energy difference between those of the relaxed considered hydride and the weighted energy of the H_2 molecule and pure *hcp*-Hf. The enthalpy was corrected with the zero point energy (ZPE) contribution. This energy is associated with the fluctuations of atom positions at 0 K and was determined by phonon calculations in the harmonic approximation (HA) using supercell approach with [38] Phonopy code.

To ensure that the calculation of the new phase is consistent with those of the previous phases, all ordered phases located in the ground state have been recalculated (PtS, NbH, ThH_2, CaF_2 and HoD_3 prototypes). Moreover the new δ'–HfH_x phase detailed later in this paper has been considered in the *Ibam* (72) space group, built on the CaF_2 with $a \times a' \times 2a$ model. Three fully ordered compositions have been considered with x=1, 1.5 and 2, corresponding to hydrogen in sites 8*g*, 4*a*+8*g* (equivalent to 4*b*+8*g*), and 4*a*+4*b*+8*g*, respectively.

4. Results

Different samples at H/Hf and D/Hf around 1 were synthesized directly at 400 °C. Three ND experiments were carried out, see Fig. 1. The first experiment was designed in order to study the low deuterium concentration range at a quasi-constant composition up to the highest possible temperature. Then, the sample was fully desorbed, and it was studied as a function of composition in isothermal conditions at 700°C, then cooled down to room temperature. The second experiment consisted in the measurement of an isotherm at 250°C. After complete charging up to D/Hf=2, the sample was heated up to 500°C. A last measurement was done at 205°C. The last experiment consisted in heating and cooling a previously synthesized sample of composition $HfD_{0.994}$ corresponding to the composition of the γ phase.

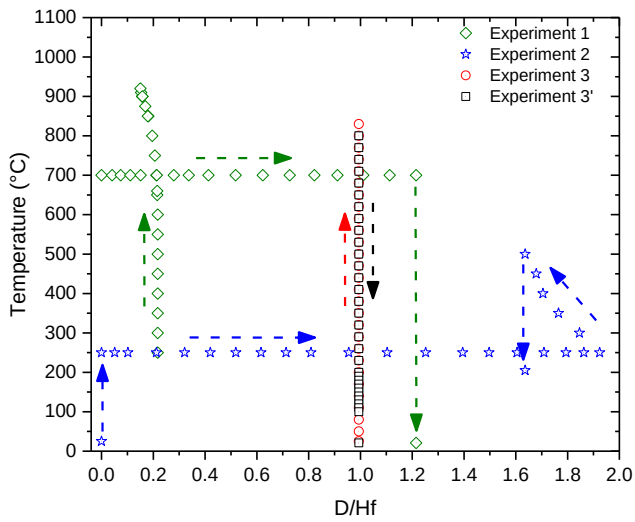

Figure 1. Sketch of the different ND experiments. Each symbol representing a given composition and temperature corresponds to the acquisition of a ND pattern.

4.1. The γ-HfH(D) phase

This phase was obtained both *ex situ* by XRD (HfH) and by ND (HfD). This confirms the prediction made by systematic high-throughput DFT calculations [7]. The decomposition temperature as observed in the *in situ* experiment is 170°C. The prototype of this tetragonal phase is PtS (space group $P4_2/mmc$, Hf in 2*c* (0,1/2,0), H-D in 2*e* (0,0,1/4). This model was chosen over the NbH prototype since a better refinement is obtained (R_B=7% compared to 38% for NbH structure). The lattice parameters at room temperature are *a* = 3.1965(4) Å and *c* = 4.7907(11) Å. Site 2*c* is considered to be fully occupied by Hf, the refined occupancy of D in site 2*e* is 1.76(4). The associated displacement parameters are 0.47(6) $Å^2$ and 0.79(15) $Å^2$, respectively.

4.2. The δ'-$HfH(D)_{2-x}$

In several diffraction patterns, the δ phase is accompanied by additional peaks. These are visible in XRD patterns but are much more intense in ND patterns. Indexation was performed with FOX, supposing that they correspond to a superstructure of the CaF_2 structure of the δ phase. They were successfully indexed with a tetragonal cell $a \times a \times 2a$. However, a pattern matching in *I*4 space group revealed that one peak remained non indexed in the ND pattern (at 49.35°) while several are slightly displaced (at 17.6°, 35.8° and 38.6°) revealing an additional orthorhombic distortion $a \times a' \times 2a$. This was never detected in the previous literature.

Extinctions can be well described in *Imcb* space group which is eventually transformed in the standard description *Ibam* by permutation. Starting from the CaF_2 structural model, it was possible to refine the structure showing both slight displacement of Hf compared to the ideal positions (explaining the low intensity superstructure peaks in the XRD patterns) and partial occupancy of deuterium sites. Two of them (8*g* and 4*b*) are nearly fully occupied while one (4*a*) is almost empty. Vacancy ordering in the non-stoichiometric HfD_{2-x} is therefore responsible for the superstructure. The ideal (fully ordered) composition with full occupancy of 8*g* and 4*b* and no occupancy in 4*a* would correspond to $HfD_{1.5}$ composition.

The Rietveld plot of a ND pattern is given in Fig. 2. The description of the structure is in Table 2 while a drawing is shown in Fig. 3.

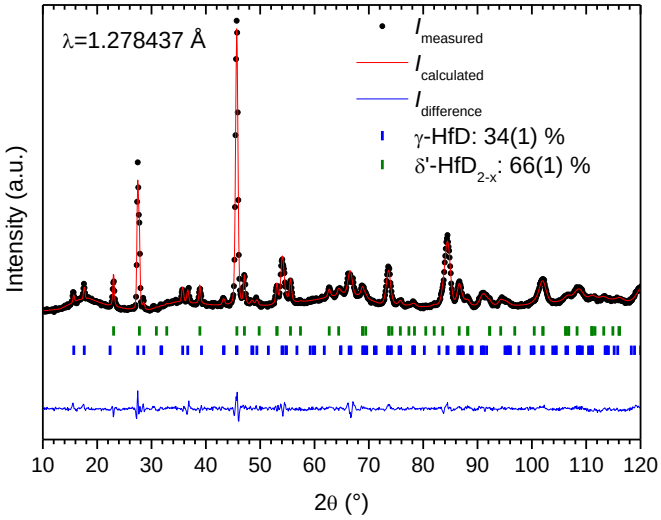

Figure 2. ND pattern of $HfD_{1.215}$ at room temperature. The measured ND pattern (points) is shown with the calculated (line) and difference (line below) curves. The vertical bars represent the reflections corresponding to the two present phases (γ and δ'). The waves in the background are due to the amorphous silica container.

Table 2. Atomic coordinates of the fully characterized δ'–$HfD_{1.44}$, *Ibam* (72) with *a* = 4.6581(7) Å; *b* = 9.3632(13) Å and *c* = 4.6239(5) Å at 25 °C.

Atom	***x***	***y***	***z***	**Site**	**Symmetry**	**Occupancy (atom)**	**Displacement parameters (Å^2)**
Hf	0.2337 (9)	0.1197 (6)	0	8*j*	..m	8	0.54 (5)
D	0	0.2554 (8)	1/4	8*g*	.2.	7.6 (1)	1.05 (6)
D	1/2	0	1/4	4*b*	222	3.59 (7)	1.05 (6)
D	0	0	1/4	4*a*	222	0.35 (6)	1.05 (6)

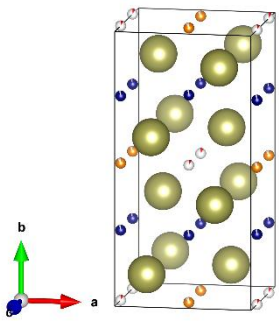

Figure 3. Structure of the δ'-HfD_{2-x} phase where the yellow balls represent the hafnium atoms, and the blue, orange and red balls represent the deuterium atoms in position 8*g*, 4*b* and 4*a*, respectively, in the form of pie charts according to the site occupancies.

4.3. Laboratory XRD

The characterization of the samples prepared *ex situ* and studied by XRD is given in Table S1. Similar results are obtained on hydrides and deuterides. The fact that three phases are observed simultaneously is similar to what is observed in H–Zr system [39-41] and can be attributed to either the effect of impurities (we are no longer in a binary system) or kinetic difficulties to reach equilibrium

4.4. *In situ* powder ND experiments

4.4.1. Experiment 1

Experiment 1 consisted in two different sequences. Hafnium powder was deuterated *in situ* up to $HfD_{0.217}$ and this sample was heated in the beam up to 920°C to check the shrinking between α and δ phases as reported previously in the literature [24, 25, 27].

Then, the sample was fully desorbed under dynamic vacuum and the deuterium composition was increased step by step along an isotherm at 700°C. The results are presented in Figs. 4 to 7 and Figs. S1 to S4.

The increase of temperature does not affect the phase ratio. From 800°C, the sample starts to desorb *i.e.* at a constant volume the pressure starts to increase which promotes the displacement of the global composition towards the α phase. The lattice parameters of the α phase increase regularly (Fig. S1) corresponding to a thermal expansion higher than that found in Refs. [11, 42] for pure Hf. For the δ phase, the decrease of the lattice parameter (Fig. 5) is related to the change of composition induced by the shrinkage of the two-phase domain in the phase diagram (decrease of the deuterium composition of the δ phase in equilibrium with α). This is clearly seen in the refined deuterium occupancy on the same figure.

On the 700°C isotherm, phase amount is shown in Fig. 6. The lattice parameters of the α phase increase significantly in the single phase domain and slightly in the two phase domain. In the same way, for the δ phase both lattice parameters and deuterium occupancy increase slightly in the two phase region, which should not be the case in equilibrium conditions.

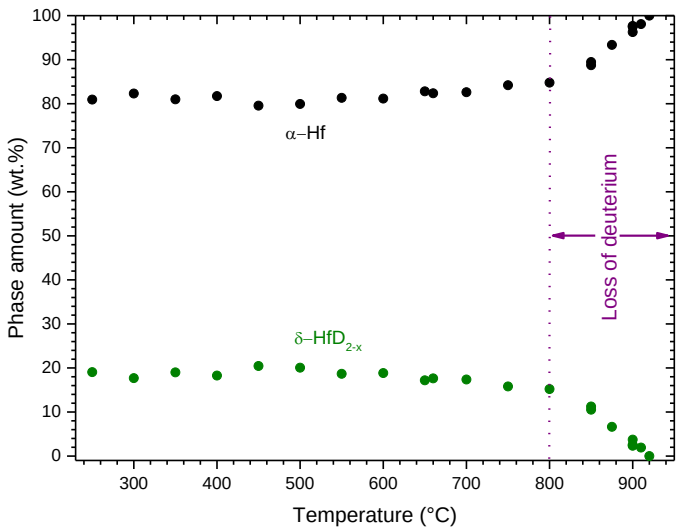

Figure 4. Phase amount of α and δ phases as a function of temperature in a sample of initial composition $HfD_{0.217}$ (experiment 1). Error bars (~1%) are commensurate with the symbol size.

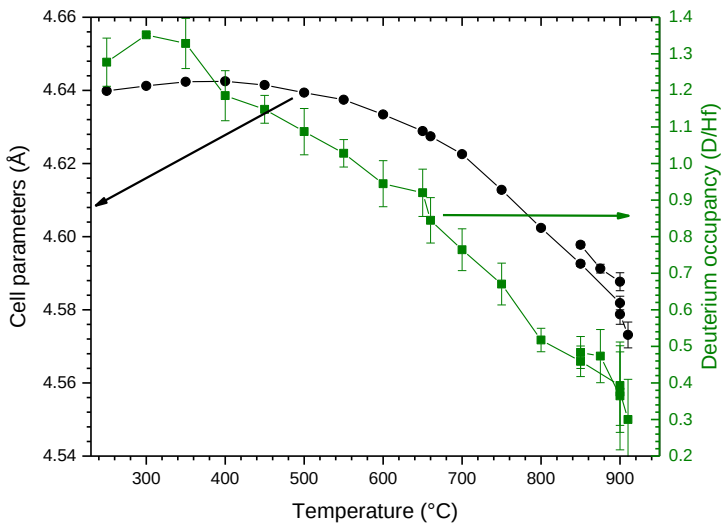

Figure 5. Cell parameter and deuterium occupancy of the δ-HfD_{2-x} phase as a function of temperature in a sample of initial composition $HfD_{0.217}$ (experiment 1). For cell parameters, error bars (0.001 Å) are commensurate with the symbol size.

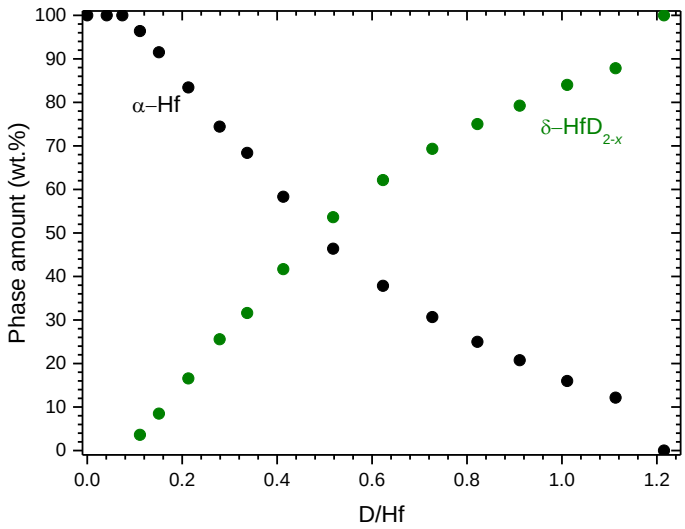

Figure 6. Phase amount as a function of overall deuterium content at 700 °C (experiment 1). Error bars (~1%) are commensurate with the symbol size.

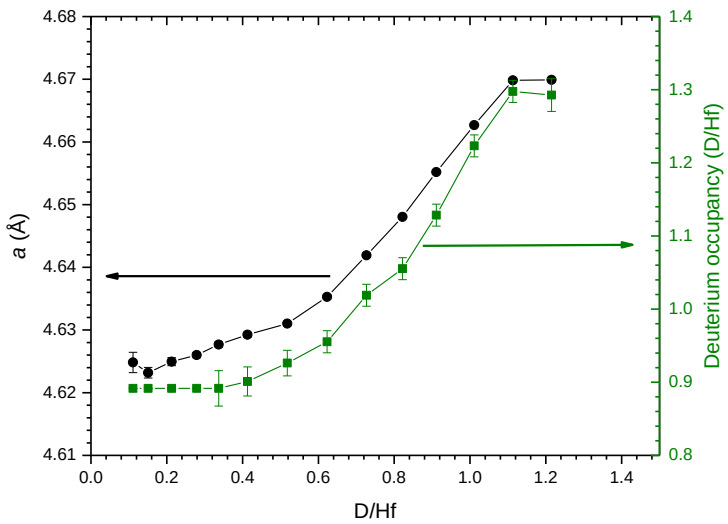

Figure 7. Cell parameter and deuterium occupancy of δ-HfD_{2-x} phase as a function of overall deuterium content at 700 °C (experiment 1). For cell parameters, error bars (0.001 Å) are commensurate with the symbol size.

4.4.2. Experiment 2

Experiment 2 consisted in an *in situ* isothermal loading of pure hafnium at 250°C. When the capacity reached 2 D/Hf, the hydride was heated up to 500°C then put under vacuum and cooled down at the same time.

During the isothermal measurement, phase amounts of α and δ phases changed until the δ phase is single phase from the composition $HfD_{1.395}$ (Fig. 8). The lattice parameters of the α phase change in the low concentration range according to a solid solution behavior and then stay constant

in the two-phase domain (Fig. S5). At high deuterium concentration, the δ phase eventually transforms into the tetragonal ε phase which lattice parameters are observed to change with composition (Fig. 9). These results are similar to these of previous literature [9, 10, 13, 15].

Fig. 10 presents the evolution of the neutron diffraction patterns as a function of composition and then as a function of temperature in the stability range of δ and ε phases (see also Fig. S6). During heating, the sample desorbs so the composition cannot be kept constant. At 250°C, between $HfD_{1.795}$ and $HfD_{1.846}$, the two phases coexist demonstrating that the transformation is of the first order in agreement with the recent finding of Bannenberg *et al.* [16].

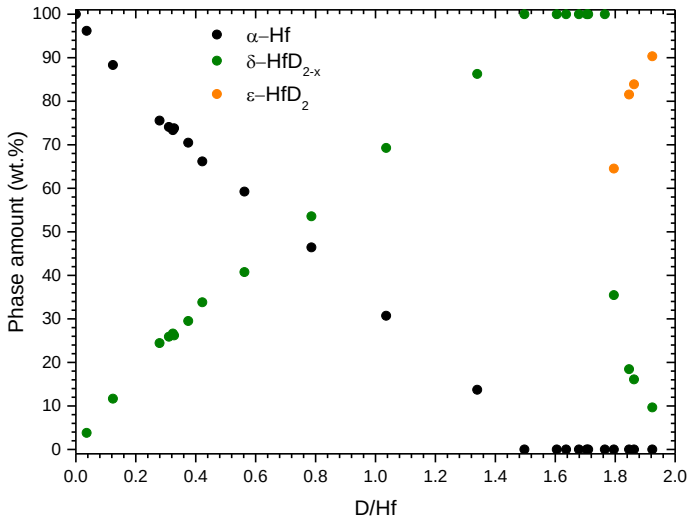

Figure 8. Phase amount as a function of overall deuterium content at 250 °C (experiment 2). Error bars (~1%) are commensurate with the symbol size.

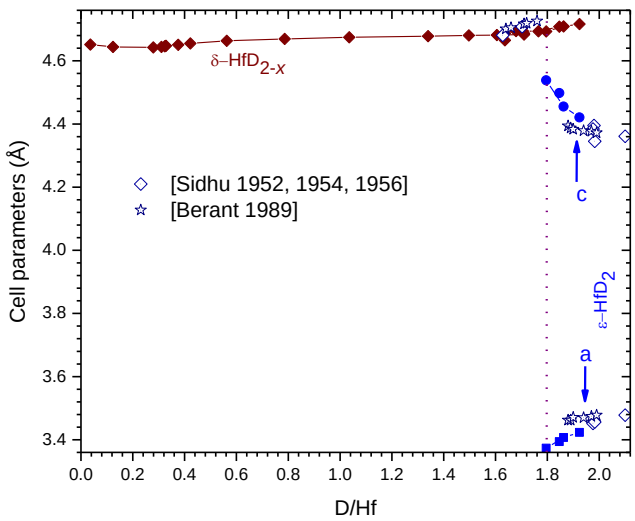

Figure 9. Cell parameters of δ-HfD_{2-x} and ε-HfD_2 phases as a function of overall deuterium content at 250 °C compared with Refs. [9, 10, 13, 15] (experiment 2). Error bars (0.001 Å) are smaller than the symbol size.

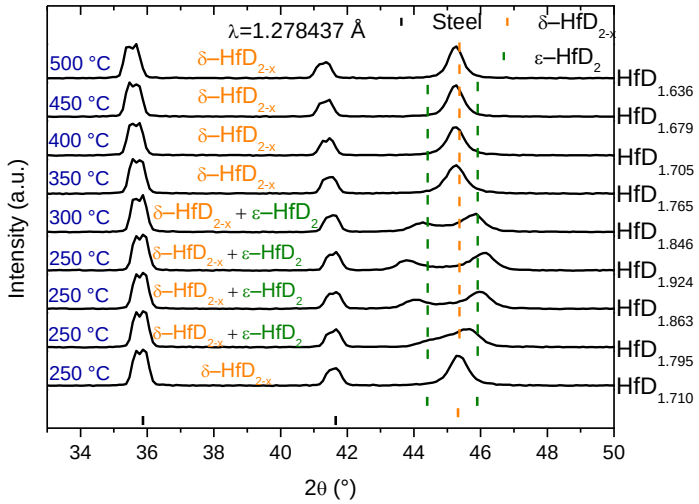

Figure 10. ND patterns of samples of different compositions at different temperatures during Experiment 2.

4.4.3. Experiment 3

This experiment consists in heating then cooling a sample of composition $HfD_{0.994}$ previously prepared. The changes of phase amount are similar during heating or cooling (Fig. 11). The amount of γ and δ phases evolve in an anti-correlated way while the amount of α is almost constant. The γ phase disappears or reappears at 170°C during heating or cooling, respectively. At low temperature, the previously identified δ' phase is observed. During heating, it transforms into the δ between 80°C and 110°C (Fig. S7). During cooling, it reappears below 100°C.

The refinement of the structural model of the δ' phase show a progressive convergence of both atomic coordinates and occupancies toward those in the CaF_2 structure when the temperature increases (Fig. 12). The progressive transformation and the apparent absence of a coexistence between δ and δ' is in favor of a second order transition as postulated in the previous literature [18, 21].

Cell parameters of the α phase increase with temperature (Fig. S8), a slight hysteresis being observed. This is similar for the δ phase (Fig. 13) except that an inversion is observed below 200°C also related to the precipitation of the γ phase and above 700°C related to the changes of composition as testified by the refinement of deuterium site occupancies. Displacement parameters are shown in Fig. S9. An example of a ND diagram is shown in Fig. S10.

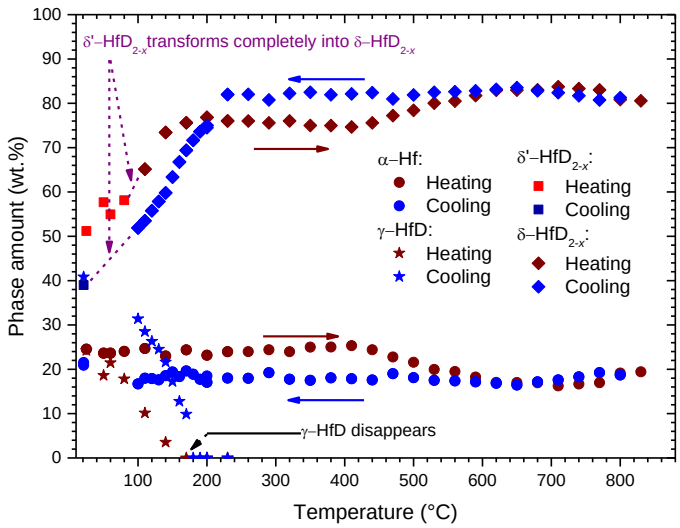

Figure 11. Phase amount as a function of temperature in a sample of initial composition $HfD_{0.994}$ (experiment 3). Error bars (~1%) are commensurate with the symbol size.

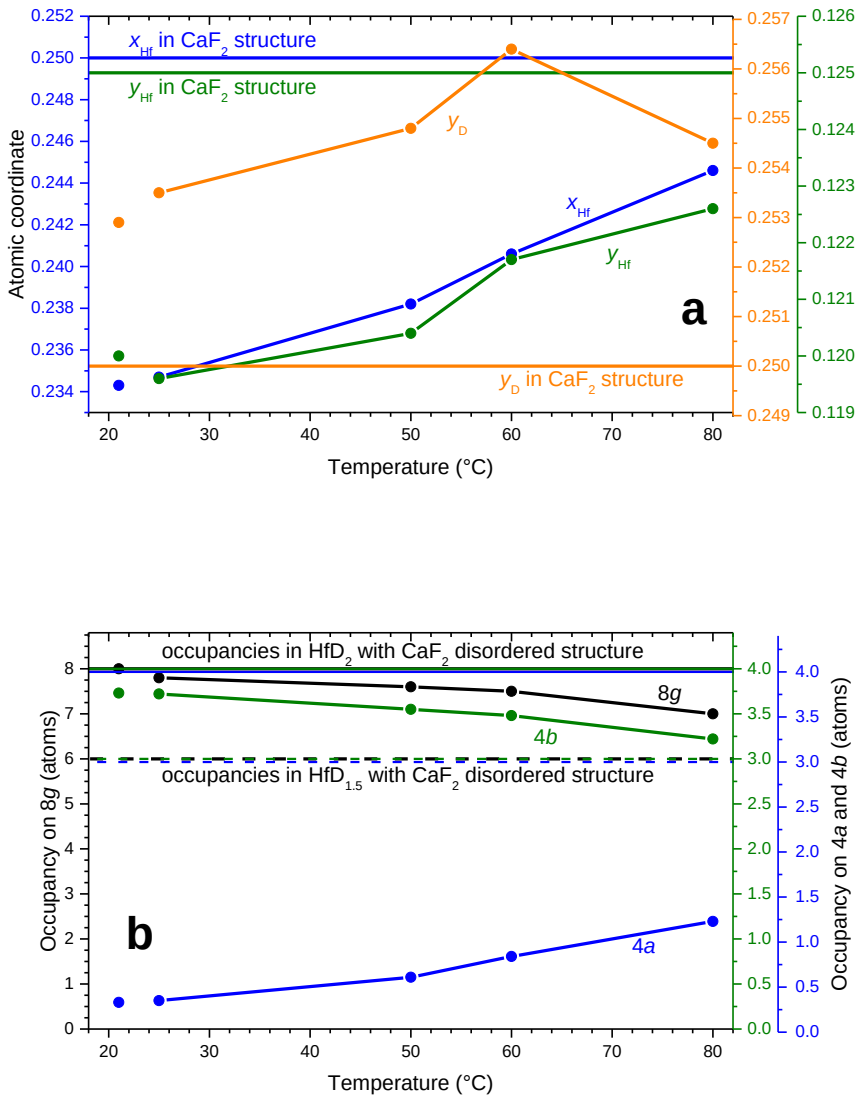

Figure 12. Atomic coordinates (a) and occupancies (b) of the δ'-HfD_{2-x} phase as a function of temperature in a sample of initial composition $HfD_{0.994}$ (experiment 3).

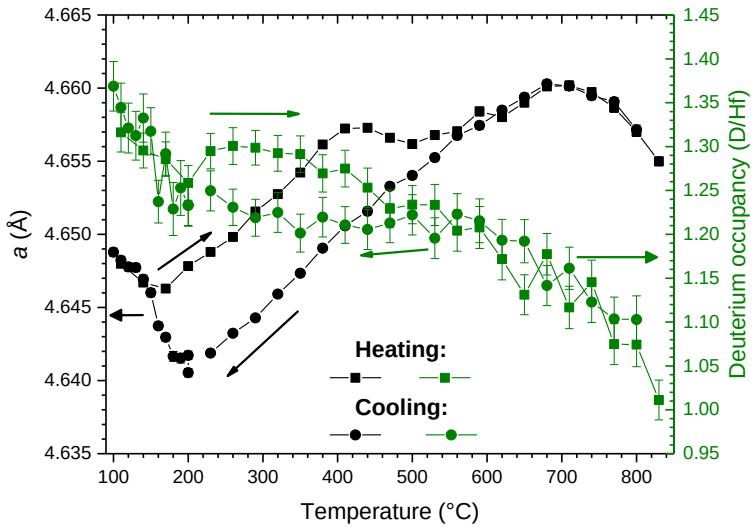

Figure 13. Cell parameters and deuterium occupancy of δ-HfD_{2-x} as a function of temperature in a sample of initial composition $HfD_{0.994}$ (experiment 3). For cell parameters, error bars (0.001 Å) are commensurate with the symbol size.

5. Discussion

5.1. γ phase

This phase has never been identified before in this system, though it is well known to form in the isoelectronic H–Zr system. It was predicted after high-throughput DFT calculations [7]. We confirmed the presence of this phase experimentally for the first time. The refinement is in favor of the tetragonal PtS over the orthorhombic NbH prototype though the energetic and crystallographic differences between the two structures are very small. As in the Zr system, the phase could never be isolated and is always observed in three phase mixtures [39, 43]. For the Zr system, this was not really explained but this did not prevent to consider it as an equilibrium phase. Finally, we noticed an anomaly during cooling between 210 °C and 150 °C where some additional peaks very close to the γ–HfD phase can be observed in our ND patterns, but they disappeared when the temperature is below 150 °C. This anomaly cannot be fully explained in this work.

5.2. δ' phase

This phase was reported to be a tetragonal phase with lattice constants and structure very close to the cubic δ-HfD_{2-x} phase. Moreover, the second order transition with the increase of the temperature between δ'-HfD_{2-x} and δ-HfD_{2-x} was estimated between 110 °C and 120 °C [18].

The structure was fully determined and refined in the present work for the first time. It is shown to be orthorhombic in contrast with the previous reports. It is a superstructure of the CaF_2 type of HfH_2 compound obtained by ordering of vacancies on the interstitial tetrahedral site when

the phase has significant substoichiometry and when the temperature is low enough (below 100°C). The order-disorder transition is confirmed to be of the second order. The drawing in Fig. S11 allows to compare the two structures.

The site with weak D occupancy (4*a*) form chains of vacancies. Wang *et al.* who made DFT calculation on atomic positions in a deformed structure δ-$HfH_{1.5}$ has also shown that neighboring vacancies were energetically favorable. Since the ordering is between hydrogen (deuterium) and vacancies, it should not be seen in principle with X-rays. However, small additional diffraction lines are visible which are explained by slight displacement of Hf atoms caused by the ordering. Only one known prototype Li_3FeN_2 has a similar crystal structure [44]. Our compound being binary, it represents therefore a new prototype.

We could modify the DFT ground state of the system as calculated by Bourgeois *et al.* [7] at $HfH_{1.5}$ composition by adding a calculation made of this new ordered compound considering complete order (full occupancy of sites 4*b* and 8*g*, no occupancy in site 4*a*), Fig. 14. The new compound is indeed found on the ground state. It is an additional proof of both the stability of this ordered phase and of the validity of the crystal structure.

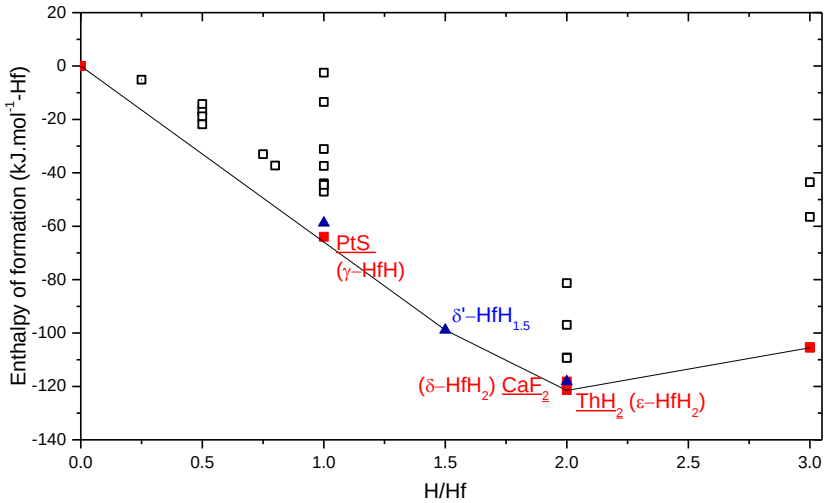

Figure 14. H–Hf ground-state calculated by DFT including ZPE correction in this work. The 3 triangles correspond to the calculations of the new δ'-HfH_x at the compositions *x*=1, 1.5 and 2, with hydrogen occupying 8*g*, 4*a*+8*g* (or 4*b*+8*g*), and 4*a*+4*b*+8*g*, respectively.

5.3. Equilibrium

It is evident that in some of the measurements, equilibrium was not reached (presence of three phases at the same time, change of the lattice parameters as a function of composition in a two-phase domain…). The time allowed to wait for equilibrium in such ND *in situ* experiment is

necessarily limited compared to usual laboratory experiments. Additionally, these are typical features of metal hydrogen systems and already noticed in many different systems.

For example, the fact that the lattice parameters increase while in a two-phase domain has been observed for long and attributed to strains between the solid solution phase and coherent hydride phases. This is also responsible for the hysteresis phenomenon. In H–Zr system, the γ-phase has been concluded to be an equilibrium phase [12, 45] though it could never be obtained as a single phase.

Altogether, these features may explain that several samples with the same compositions at the same temperatures in different experiments were not absolutely reproducible, for example, between an isothermal measurement and a temperature increase at a given composition. For example, if we compare the results obtained at 250°C for the sample $HfD_{0.217}$ in experiment 1 (where the temperature increased) and the sample $HfD_{0.2127}$ of the experiment 2 (where PCI was measured), one can see that the amount of α phase refined is 80.9 % versus 75.6 %, respectively.

Additionally, our system is not strictly binary due to the presence of ~5 at.% Zr (purest material is not available commercially), though we do not believe that this could have a large influence on the phase diagram.

5.4. Pressure-composition isotherms

Our *in situ* measurement of the deuterium pressure-composition isotherms at 700 °C (experiment 1), at 250 °C (experiment 2) and the measurements made above 600 °C (experiment 3) are shown and compared with the literature data in Fig. 15. As indicated above, according to the calorimetric data at 334 K in Ref. [28], no isotopic effect was expected. However, a strong inverse isotopic effect between H and D is observed as far as the plateau pressure is concerned (higher equilibrium pressure for the D–Hf system) (see Fig. 16). The discrepancy with the calorimetric measurement of Ref. [28] is not explained.

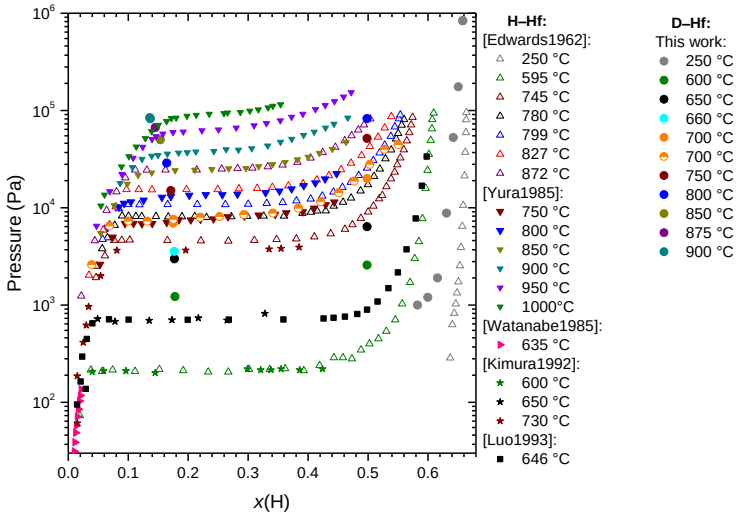

Figure 15. Pressure-composition absorption isotherms measured at several temperatures obtained in this work for D–Hf and in Refs. [24-28] for H–Hf. Error bars for our measurement is about 500 Pa.

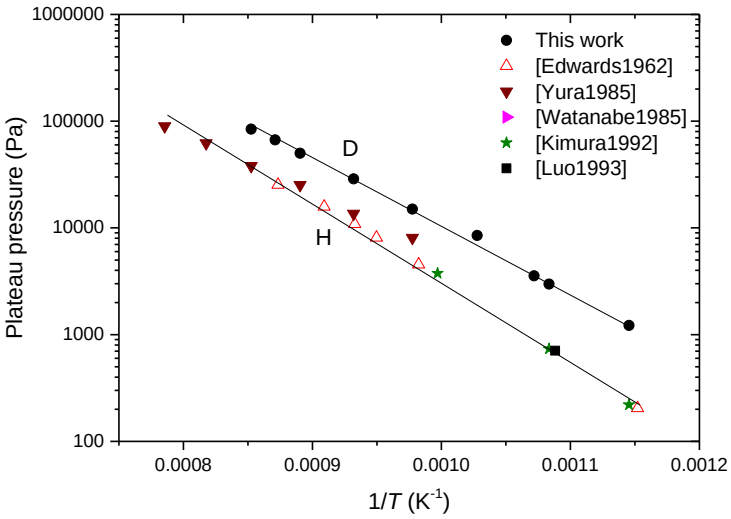

Figure 16. α–δ plateau pressure as a function of the inverse temperature from the literature [24, 25, 27, 28] (hydrogen) and from this work (deuterium). Lines are drawn to guide the eyes.

5.5. Phase diagram

We can synthesize our results with the plot of a new phase diagram of H–Hf system. For the phase compositions, it is difficult to choose between those measured experimentally from the Sieverts' method, those obtained from the lattice parameter variations, those from the phase fractions and those obtained by a structural refinement of the deuterium occupancies. The latter was finally chosen. The plot is essentially based on our measurements. Formally, it is relative to deuterium rather than hydrogen. No major difference is expected between D–Hf and H–Hf systems as long as equilibrium between solid phases is considered. For the equilibrium with the gas phase,

due to the isotopic effect discussed above, lower solubilities are expected with deuterium and lower temperature for the invariant points are expected. The solubilities change also with pressure and, according to our measurements, the plot is done at ~1 bar and ~9 bar. It is complemented by literature data for the compositions of the δ and ε phases.

An excellent agreement is observed between our measurement of the transition temperature between δ' and δ and literature [19, 21], and for the phase limits in the region D/Hf > 1.5, T < 300 °C. Slight discrepancies between our α solvus and the literature [24, 25] may be attributed to the fact that our measurement is from the refinement of the site occupancies instead of pressure-composition curves. Such a discrepancy is not observed for the δ solvus in equilibrium with α for which the composition from the structural refinement is in perfect agreement with the pressure-composition measurements from Edwards and Veleckis [24]. For the equilibrium with gas, the discrepancy is due to the isotope effect.

New features of the phase diagram of Fig. 17 compared to past descriptions can be listed:

- presence of an additional γ phase with peritectoid formation
- confirmation of the existence of the δ' phase with a new crystal prototype and a second order transition towards the δ phase
- determination of the formation temperature of the ε phase by a gas-peritectic reaction and confirmation of the first order transition with the δ phase as already observed in Ref. [16]
- clarification of the drawing in the region 1.8 < D/Hf < 2
- better characterization of the δ phase limits in equilibrium with α and with gas

As in previous work, no inflexion of the δ solvus in equilibrium with α could be seen up to the highest temperature we could reach (limited by the significant pressure and the risk of explosion of the silica tube) and down to the lowest deuterium composition (23 at.%). As such, it would cross the α solvus and extrapolate to an *hcp* to *fcc* allotropic phase transition for pure hafnium around 1000°C. This is also one of the reason why our α solvus is more credible than that obtained from the pressure-composition curves. Evidently, such a transition has never been seen, so the solvus should change its behavior above 900°C, but it should be noted that *fcc* Hf has been observed as a metastable phase in Hf–Mg alloys [46] and even for pure Hf [47]. All these results indicates that the *fcc* Hf is indeed quite close to stability compared to the stable *hcp* Hf.

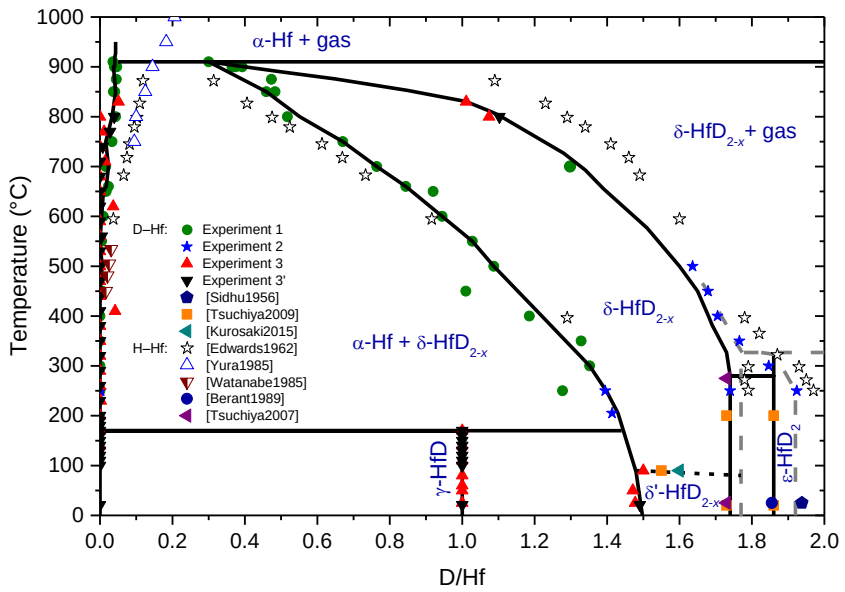

Figure 17. Phase diagram of H–Hf(D–Hf) system obtained in this work drawn at *p*=1 bar (in dashed *p*=9 bar). Literature data is from Refs. [10, 15, 17, 19, 21, 24-26].

5.6. Comparison with H–Zr system

A comparison with H–Zr system is interesting because Hf and Zr are isoelectronic and the hydrides of both systems have applications in the nuclear industry. Many features are common between the two systems like the allotropic forms, α and β, of the pure element and the existence of the hydrides γ, δ and ε.

However, differences can be observed. These are mainly related to the difference of the melting and allotropic transformation temperatures which are much higher in the case of Hf. For this reason, the stabilizing effect of hydrogen on the β phase could not be verified in the case of Hf. It is likely that, at the temperature the β phase will be stable, the hydrogen solubility will be extremely low at moderate pressure. The solubility in the α phase is slightly lower in Hf system (4.4 at.% at 900°C) than in Zr system (6 at.% at 550°C). Other very striking difference is the stability of the δ phase in the Hf system at very low compositions contrary to Zr system in which it only slightly departs from the ideal ZrH_2 stoichiometry. Also related to the non-stoichiometry, the ordering of the δ phase is another typical feature of the Hf system.

The γ phase is less stable in the H–Hf system. Moreover, the α-δ plateau pressures are lower in H–Zr system than in H–Hf system.

6. Conclusion

An *in situ* neutron diffraction experiment has been carried out in D–Hf system as a function of both temperature and composition. The presence of the γ phase anticipated in our previous DFT

study has been confirmed experimentally. The crystal structure of the ordered δ' phase has been solved. A DFT calculation shows that the phase is indeed present on the ground state of the system. Finally, combined with literature data, a new phase diagram of the system could be plotted.

ACKNOWLEDGEMENTS

ILL is acknowledged for beamtime allocation and we would like to thank Vivian Nassif and Inés Puente Orench from Institut Néel for assistance in using CRG-D1B. Fabrice Couturas from ICMPE is acknowledged for help with ND at ILL. DFT calculations were performed using HPC resources from GENCI-CINES (Grant 2021-A0100906175)

DECLARATION OF INTERESTS

The authors declare that they have no known competing financial interests or personal relationships that could have appeared to influence the work reported in this paper.

REFERENCES

[1] G. Ek, M. M. Nygård, A. F. Pavan, J. Montero, P. F. Henry, M. H. Sørby, M. Witman, V. Stavila, C. Zlotea, B. C. Hauback and M. Sahlberg, *Inorg. Chem.*, 60 (2021) 1124-1132.
[2] C. Boelsma, L. J. Bannenberg, M. J. van Setten, N.-J. Steinke, A. A. van Well and B. Dam, *Nature Commun.*, 8 (2017) 15718.
[3] V. D. Risovanyi, E. P. Kloshkov and E. E. Varlashova, *Atom. Energy*, 81 (5) (1996) 764-769.
[4] T. Iwasaki and K. Konashi, *J. Nucl. Sci. Technol.*, 46 (8) (2009) 874-882.
[5] Y. Tahara, T. Iwasaki and K. Konashi, *J. Nucl. Sci. Technol.*, 47 (4) (2010) 421-429.
[6] K. Ikeda, H. Moriwaki, Y. Ohkubo, T. Iwasaki and K. Konashi, *Nucl. Eng. Des.*, 278 (2014) 97-107.
[7] N. Bourgeois, J.-C. Crivello, P. Cenedese and J.-M. Joubert, *ACS Comb. Sci.*, 19 (2017) 513-523.
[8] M. Latroche, P. H. L. Notten and A. Percheron-Guégan, *J. Alloys Compd.*, 253-254 (1997) 295-297.
[9] S. S. Sidhu, *Acta Crystallogr.*, 7 (1954) 447-449.
[10] S. S. Sidhu, L. Heaton and D. D. Zauberis, *Acta Crystallogr.*, 9 (1956) 607-614.
[11] P. A. Romans, O. G. Paasche and H. Kato, *J. Less-Common Met.*, 8 (3) (1965) 213-215.
[12] F. Long, N. N. Badr, Z. Yao and M. R. Daymond, *J. Nucl. Mater.*, 543 (2021) 152540.
[13] S. S. Sidhu and J. C. McGuire, *J. Appl. Phys.*, 23 (11) (1952) 1257-1261.

[14] R. A. Andrievskii, V. I. Savin and R. A. Lyutikov, *Russ. J. Inorg. Chem.*, 17 (4) (1972) 477-479.
[15] Z. Berant, Y. Levitin, S. Kahane, A. Wolf and M. H. Mintz, *Hyperfine Interact.*, 52 (4) (1989) 383-397.
[16] L. J. Bannenberg, H. Schreuders, H. Kim, K. Sakaki, S. Hayashi, K. Ikeda, T. Otomo, K. Asano and B. Dam, *J. Phys. Chem. Lett.*, 12 (2021) 10969-10974.
[17] B. Tsuchiya, M. Teshigawara, K. Konashi, S. Nagata and T. Shikama, *J. Alloys Compd.*, 446-447 (2007) 439-442.
[18] Y. Arita, T. Ogawa, B. Tsuchiya and T. Matsui, *J. Therm. Anal. Calorim.*, 92 (2) (2008) 403-406.
[19] B. Tsuchiya, Y. Arita, H. Muta, K. Kurosaki, K. Konashi, S. Nagata and T. Shikama, *J. Nucl. Mater.*, 392 (2009) 464-470.
[20] H. Wang and K. Konashi, *J. Nucl. Mater.*, 443 (2013) 99-106.
[21] K. Kurosaki, D. Araki, Y. Ohishi, H. Muta, K. Konashi and S. Yamanaka, *J. Nucl. Sci. Technol.*, 52 (4) (2015) 541-545.
[22] O. M. Katz and J. Alfred Berger, *Trans. Metall. Soc. AIME*, 233 (1965) 1005-1013.
[23] S. Yamanaka, H. Ogawa and M. Miyake, *J. Less-Common Met.*, 172-174 (1991) 85-94.
[24] R. K. Edwards and E. Veleckis, *J. Phys. Chem.*, 66 (9) (1962) 1657-1661.
[25] K. Yura, S. Naito, M. Mabuchi and T. Hashino, *J. Chem. Soc. Faraday T2*, 82 (1985) 101-114.
[26] K. Watanabe, *J. Nucl. Mater.*, 136 (1985) 1-5.
[27] M. Kimura, S. Naito, M. Mabuchi and T. Hashino, *J. Chem. Soc. Faraday T*, 88 (15) (1992) 2221-2226.
[28] W. Luo, T. B. Flanagan, J. D. Clewley and P. Dantzer, *Metall. Trans. A*, 24A (1993) 2623-2627.
[29] F. Ricca and T. A. Giorgi, *J. Phys. Chem.*, 74 (1) (1970) 143-146.
[30] L. Espagno, P. Azou and P. Bastien, *C. R. Acad. Sci., Paris*, 250 (1960) 4352-4354.
[31] H. M. Rietveld, *J. Appl. Crystallogr.*, 2 (1969) 65–71.
[32] J. Rodríguez-Carvajal, *Commission on Powder Diffraction, Newsletter*, (26) (2001) 12-19.
[33] V. Favre-Nicolin and R. Cerný, *J. Appl. Crystallogr.*, 35 (2002) 734-743.
[34] G. Kresse and J. Furthmüller, *Phys. Rev., B*, 54 (1996) 11169-11186.
[35] J. P. Perdew, K. Burke and M. Ernzerhof, *Phys. Rev. Lett.*, 77 (18) (1996) 3865-3868.
[36] G. Kresse and D. Joubert, *Phys. Rev., B*, 59 (3) (1999) 1758-1775.
[37] H. J. Monkhorst and J. D. Pack, *Phys. Rev., B*, 13 (1976) 5188-5192.
[38] A. Togo and I. Tanaka, *Scr. Mater.*, 108 (2015) 1-5.
[39] Z. Wang, A. Steuwer, N. Liu, T. Maimaitiyili, M. Avdeev, J. Blomqvist, C. Bjerkén, C. Curfs, J. A. Kimpton and J. E. Daniels, *J. Alloys Compd.*, 661 (2016) 55-61.
[40] T. Maimaitiyili, C. Bjerken, A. Steuwer, Z. Wang, J. Daniels, J. Andrieux, J. Blomqvist and O. Zanellato, *J. Alloys Compd.*, 695 (2017) 3124-3130.
[41] T. Maimaitiyili, A. Steuwer, C. Bjerkén, J. Blomqvist, M. Hoelzel, J. C. Ion and O. Zanellato, *J. Nucl. Mater.*, 485 (2017) 243-252.
[42] R. G. Ross and W. Hume-Rothery, *J. Less-Common Met.*, 5 (3) (1963) 258-270.
[43] T. Maimaitiyili, J. Blomqvist, A. Steuwer, C. Bjerkén, O. Zanellato, M. S. Blackmur, J. Andrieux and F. Ribeiro, *J. Synchrotron Radiat.*, 22 (2015) 995-1000.
[44] N. Emery, M. T. Sougrati, E. Panabière, S. Bach, B. Fraisse, J.-C. Jumas, J.-P. Pereira-Ramos and P. Willmann, *J. Alloys Compd.*, 696 (2017) 971-979.
[45] Xueyan Zhu, De-Ye Lin, Jun Fang, Xing-Yu Gao, Ya-Fan Zhao and Hai-Feng Song, *Comput. Mater. Sci.*, 150 (2018) 77-85.
[46] E. I. López Gómez, K. Edalati, D. D. Coimbrão, F. J. Antiqueira, G. Zepon, J. M. Cubero-Sesin and W. J. Botta, *AIP Adv.*, 10 (2020) 055222.
[47] U. M. R. Seelam and C. Suryanarayana, *J. Appl. Phys.*, 105 (2009) 063524.